

LETTER TO THE EDITOR

# Investigating source confusion in PMN J1603–4904

F. Krauß<sup>1</sup>, M. Kreter<sup>2</sup>, C. Müller<sup>3</sup>, A. Markowitz<sup>4,5</sup>, M. Böck<sup>6</sup>, T. Burnett<sup>7</sup>, T. Dauser<sup>6</sup>, M. Kadler<sup>2</sup>, A. Kreikenbohm<sup>2</sup>,  
R. Ojha<sup>8</sup>, and J. Wilms<sup>6</sup>

<sup>1</sup> GRAPPA & Anton Pannekoek Institute for Astronomy, University of Amsterdam, Science Park 904, 1098 XH Amsterdam, The Netherlands

e-mail: Felicia.Krauss@uva.nl

<sup>2</sup> Institut für Theoretische Physik und Astrophysik, Universität Würzburg, Emil-Fischer-Str. 31, 97074 Würzburg, Germany

<sup>3</sup> Department of Astrophysics/IMAPP, Radboud University Nijmegen, Heyendaalseweg 135, 6525 AJ Nijmegen, Netherlands

<sup>4</sup> Nicolaus Copernicus Astronomical Center, Polish Academy of Sciences, Bartycka 18, PL-00-716 Warszawa, Poland

<sup>5</sup> Center for Astrophysics & Space Science, University of California, San Diego, La Jolla, CA, 92093-0424, USA

<sup>6</sup> Dr. Remeis Sternwarte & ECAP, Universität Erlangen-Nürnberg, Sternwartstrasse 7, 96049 Bamberg, Germany

<sup>7</sup> Department of Physics, University of Washington, Seattle, WA 98195-1560, USA

<sup>8</sup> NASA, Goddard Space Flight Center, Astrophysics Science Division, Code 661, Greenbelt, MD 20771, USA

Received 22 November 2017 / Accepted <date>

## ABSTRACT

PMN J1603–4904 is a likely member of the rare class of  $\gamma$ -ray emitting young radio galaxies. Only one other source, PKS 1718–649, has been confirmed so far. These objects, which may transition into larger radio galaxies, are a stepping stone to understanding AGN evolution. It is not completely clear how these young galaxies, seen edge-on, can produce high-energy  $\gamma$ -rays. PMN J1603–4904 has been detected by TANAMI Very Long Baseline Interferometry (VLBI) observations and has been followed-up with multiwavelength observations. A *Fermi*/LAT  $\gamma$ -ray source has been associated with it in the LAT catalogs. We have obtained *Chandra* observations of the source in order to consider the possibility of source confusion, due to the relatively large positional uncertainty of *Fermi*/LAT. The goal was to investigate the possibility of other X-ray bright sources in the vicinity of PMN J1603–4904 that could be counterparts to the  $\gamma$ -ray emission. With *Chandra*/ACIS, we find no other sources in the uncertainty ellipse of *Fermi*/LAT data, which includes an improved localization analysis of 8 years of data. We further study the X-ray fluxes and spectra. We conclude that PMN J1603–4904 is indeed the second confirmed  $\gamma$ -ray bright young radio galaxy.

**Key words.** galaxies: active — galaxies: jets — galaxies: individual: PMN J1603–4904

## 1. Introduction

Active Galactic Nuclei (AGN) are the most luminous persistent objects in the Universe. A subset of AGN exhibits relativistic outflows, called jets. Many questions of jet physics remain unsolved, including the details of jet launching, confinement and acceleration processes. In this context, peculiar AGN in transitory stages become relevant for addressing the key questions of AGN science. Among these objects are young radio galaxies, which exhibit shorter jets (up to a few kpc), and are also known as compact symmetric objects (CSO) due to their compactness at radio wavelengths (Phillips & Mutel 1982; Wilkinson et al. 1994; Readhead et al. 1996; O’Dea 1998). They are typically seen at large inclination angles to the jet(s) and have negligible Doppler boosting. While  $\gamma$ -ray emission from young AGN was predicted (Kino et al. 2007, 2009; Stawarz et al. 2008; Kino & Asano 2011), a detection by the *Fermi Gamma-ray Space Telescope* Large Area Telescope (hereafter *Fermi*/LAT) remained elusive for many years (D’Ammando et al. 2016). Using the improved Pass 8 reconstruction (Atwood et al. 2013), Migliori et al. (2016) detected the first CSO at  $\gamma$ -ray energies, PKS 1718–649. Three other candidate sources have been proposed: 4C +55.17 (McConville et al. 2011), PKS 1413+135 (Gugliucci et al. 2005), and PMN J1603–4904 (Müller et al. 2014). The first two have not been confirmed to be young radio galaxies. It remains unclear which attributes make some young AGN  $\gamma$ -ray loud. A di-

rect link between Narrow Line Seyfert 1 galaxies (NLS1) and young AGNs (Compact Symmetric Sources) has been suggested by Caccianiga et al. (2014), but seems unlikely (Orienti et al. 2015).

PMN J1603–4904 is a radio source (Wright et al. 1994). It was recently confirmed to be a compact symmetric object from MHz data, which makes it a young or frustated AGN (Müller et al. 2016). It was detected by *Fermi*/LAT and classified as a low synchrotron peaked (LSP) BL Lac object (2FGL J1603.8–4904, 3FGL J1603.9–4903; Nolan et al. 2012; Acero et al. 2015; Ackermann et al. 2015). The first association with the  $\gamma$ -ray source was proposed by Kovalev (2009). It is also listed in the LAT catalogs of sources detected above 10 GeV and 50 GeV (1FHL J1603.7–4903, 2FHL J1603.9–4903, 3FHL J1603.8–4903 Ackermann et al. 2013, 2016; The *Fermi*-LAT Collaboration 2017). It is reported as a variable source in the 3FGL catalog. PMN J1603–4904 was first proposed to be a  $\gamma$ -ray bright CSO by Müller et al. (2014), who discussed its unusual VLBI structure and spectral energy distribution (SED). We followed up on this paper with X-ray observations with *Suzaku* and *XMM-Newton*, which led to the first high S/N X-ray spectrum that also exhibited an emission line at 5.44 keV, which we interpreted as a redshifted neutral Fe K $\alpha$  line (at  $z = 0.18$ ; Müller et al. 2015). Optical data by Shaw et al. (2013), which resulted in the LSP BL Lac classification, were not sensitive enough to de-

tect any lines. Further optical spectroscopy showed our proposed redshift to be incorrect. X-Shooter data resulted in a redshift measurement of  $z = 0.2321 \pm 0.0004$  (Goldoni et al. 2016). The emission line is due to He-like Fe, emitted at a rest frame energy of 6.7 keV. This emission feature is not typically seen in AGN, where edge-on sources exhibit neutral or slightly ionized Fe  $K\alpha$  emission, which is expected to originate in the accretion disks. This feature seems to be common for CSO sources (Siemiginowska et al. 2016). Highly ionized Fe emission is also observed in the LINER galaxy M81 (Page et al. 2004), though the latter still exhibits neutral Fe  $K\alpha$  emission while PMN J1603–4904 does not. It is unclear whether this suggests a complete lack of an accretion disk, a truncated accretion disk (which could likely achieve the high temperatures to ionize Fe) or a lack of neutral Fe.

Further radio studies of PMN J1603–4904 find a low-frequency turnover in the MHz – GHz spectrum, which indicates a source extent of 1.4 kpc and confirmed its young radio source classification (Müller et al. 2016). The source is located close to the Galactic plane ( $l = 332^\circ 15$ ,  $b = 2^\circ 57$ ), which hinders optical/UV and soft X-ray observations due to extinction and photoelectric absorption. The low Galactic latitude also complicates  $\gamma$ -ray data analysis due to the large number of nearby sources, the Galactic diffuse emission, and the three nearby extended sources, which all have to be taken into account. The radio source is consistent with the *Fermi*/LAT 95% 2FGL positional uncertainty, but it is unclear if there are other possible counterparts within the uncertainty ellipse in either radio or X-ray wavelengths (Müller et al. 2014). Optical data are unable to solve this problem, due to the large number of nearby stars and the strong extinction. In this paper we examine recent *Chandra*/ACIS data, the highest angular resolution data available at high energies, to confirm or rule out source confusion for PMN J1603–4904. In Section 2 we discuss the observations and analysis methods. In Section 3 we discuss the results of the observations. The final section reports our conclusions.

## 2. Observations & Methods

### 2.1. Chandra

We took one *Chandra* observation of PMN J1603–4904 with the Advanced CCD Imaging Spectrometer (ACIS; observation ID 17106, 10.08 ksec) on 12 May 2016. The data are not affected by pile-up, as PMN J1603–4904 is a relatively weak X-ray emitter (Müller et al. 2015). The data were extracted using the standard tools from the CIAO 4.8. The extraction radius for PMN J1603–4904 is  $3''.3$ , while the background was extracted with annuli centered on the source position with radii of  $4''.4$  and  $40''$ . The source to the east of PMN J1603–4904 (no. 1, see Fig. 1) was extracted with an extraction radius of  $4''.9$ , while the background annulus radii were  $8''.3$  and  $25''.9$ . The source to the east is seen in archival *XMM* data as well. The source to the west is not detected in *XMM*, either due to its low flux, or it is variable. The spectral analysis was performed with the Interactive Spectral Interpretation System (ISIS, version 1.6.2-40, Houck & Denicola 2000). The *Chandra* data were modeled with an absorbed powerlaw, which fits both PMN J1603–4904 and the eastern source (no. 1). Due to low S/N in the individual bins, we use Cash statistics (Cash 1979) for spectral analysis. For the absorbing column we use the abundances of Wilms et al. (2000) and the cross sections of Verner et al. (1996) with the newest

**Table 1.** *Chandra* positions of the three X-ray sources in the direct vicinity of PMN J1603–4904 ( $\alpha_{J2000.0} = 16^{\text{h}}03^{\text{m}}50^{\text{s}}.69$ ,  $\delta_{J2000.0} = -49^\circ 04' 05''.49$ ). Positions and uncertainties have been determined using wavdetect. The position of the central source (no. 2) is consistent with the radio position of PMN J1603–4904.

| No. | $\alpha_{J2000.0}$                            | $\delta_{J2000.0}$      | $u(\alpha_{J2000.0})$ | $u(\delta_{J2000.0})$ |
|-----|---|-------------------------|-----------------------|-----------------------|
| 1   | $16^{\text{h}}04^{\text{m}}01^{\text{s}}.111$ | $-49^\circ 04' 12''.00$ | 0.139''               | 0.182''               |
| 2   | $16^{\text{h}}03^{\text{m}}50^{\text{s}}.687$ | $-49^\circ 04' 04''.44$ | 0.046''               | 0.035''               |
| 3   | $16^{\text{h}}03^{\text{m}}34^{\text{s}}.280$ | $-49^\circ 02' 57''.16$ | 0.238''               | 0.130''               |

version of the tbnew model<sup>1</sup>. In order to determine the coordinates of the X-ray sources we ran the CIAO tools `mkpsfmap` (at 2 keV with 50% enclosed counts) and `wavdetect` with the default scales. For the de-reddening of the optical/UV/IR data, the best-fit absorbing column  $N_{\text{H}}$  has been converted to  $A_{\text{V}}$  from X-ray dust scattering halo measurements of Predehl & Schmitt (1995), with the update by Nowak et al. (2012) for the revised abundance of the interstellar medium (see Krauß et al. 2016 for a detailed explanation of the treatment of multiwavelength data).

### 2.2. Fermi/LAT $\gamma$ -ray data analysis

For the analysis of the *Fermi*/LAT  $\gamma$ -ray data, we used the *Fermi* Science Tools (v11r0p0) with the reprocessed Pass 8 data and the P8R2\_SOURCE\_V6 instrument response functions. The localization of the source is tricky with `gtfindsrc` due to its position near the Galactic plane. The localization we performed is similar to that in the 3FGL catalog (Acero et al. 2015), and only data above 3.2 GeV have been used as the data have been binned 4/decade. The log-likelihood surface is assumed to be parabolic. A selection of eight points is sampled in a circle around the estimated position, which is used to estimate the five parameters for the ellipse. The center is then moved to the estimated maximum, a new circle chosen at the  $2\sigma$  radius, and the procedure is iterated until convergence. The deviation of the fit from the measured values defines a goodness-of-fit quantity. The curvature of the surface is used to determine the covariance matrix, which in turn determines the positional uncertainty ellipse. We quote the values corresponding to a 95% containment. The positions and uncertainties are then used to determine the need for systematic adjustment by comparing with a set of AGNs, which have very accurate radio positions. To account for them we multiply the 95% uncertainties by a factor of 1.05, and add  $0.433'$  in quadrature. For the spectral analysis we used an unbinned likelihood analysis in a region of interest of  $5^\circ$  around PMN J1603–4904 in the 1–300 GeV energy range. Sources within a  $15^\circ$  radius of PMN J1603–4904 were included in the likelihood fitting, with their parameters fixed. A free spectral index is used, together with a detection threshold of test statistic  $TS = 25$  (Wilks 1938).

## 3. Results

We find three X-ray sources in the *Chandra*/ACIS image in the direct vicinity of the 2MASS coordinates of PMN J1603–4904 (see Fig. 1; Skrutskie et al. 2006). The coordinates are given in Table 1. The X-ray source in the center (no. 2) matches the radio coordinates. We can exclude the western source (no. 3) as a counterpart. It is at an angular distance of  $2''.9$  to PMN J1603–4904, well outside the uncertainty ellipses of our

<sup>1</sup> available online at: <http://pulsar.sternwarte.uni-erlangen.de/wilms/research/tbabs/>

**Table 2.** Best fit values from *Suzaku* and *XMM-Newton* data taken from Müller et al. (2015) in comparison with best fit values for *Chandra*/ACIS data for PMN J1603–4904 and two fits to the eastern source. Values without uncertainties have been frozen to the given value. Uncertainties are given at the 90% confidence level. The absorbing column is given in units of  $10^{22} \text{ cm}^{-2}$ , and the unabsorbed 2–10 keV flux is given in units of  $10^{-13} \text{ erg s}^{-1} \text{ cm}^{-2}$ .

| Parameter           | <i>Suzaku</i> &        | <i>Chandra</i>         | <i>Chandra</i>         | <i>Chandra</i>        |
|---------------------|------------------------|------------------------|------------------------|-----------------------|
|                     | <i>XMM</i>             |                        | East                   | East                  |
| $N_{\text{H}}$      | $2.05^{+0.14}_{-0.12}$ | 2.05                   | 2.05                   | 0.632                 |
| $\Gamma$            | $2.07^{+0.04}_{-0.12}$ | $2.23^{+0.29}_{-0.28}$ | $5.3^{+1.5}_{-2.1}$    | $3.0^{+1.4}_{-1.2}$   |
| $F_{2-10}$          | $4.39 \pm 0.17$        | $2.8^{+0.7}_{-0.6}$    | $0.08^{+0.05}_{-0.04}$ | $0.14^{+0.28}_{-0.1}$ |
| $\chi^2/\text{dof}$ | 183.0/162              | 28.8/37                | 2.9/3                  | 2.3/3                 |

analysis and those of the *Fermi*/LAT catalogs. The eastern source (no. 1) is also outside the LAT uncertainty ellipses, but closer, being at an angular distance of  $1'7$  and the 3FGL uncertainty region seems to be closer to the eastern source than any of the LAT results (see Fig. 1, right panel). Based on this image, the  $\gamma$ -ray source is indeed the counterpart to the young radio source, although the radio source lies just outside the 3FGL 95% uncertainty ellipse. In the 8-year *Fermi*/LAT analysis, the source is detected at  $TS = 2373$ , with a photon index  $\Gamma = 1.98 \pm 0.03$  and a flux  $F_{1-300 \text{ GeV}} = (5.57 \pm 0.22) \times 10^{-9} \text{ ph s}^{-1} \text{ cm}^{-2}$ . This flux is slightly lower than the fluxes reported in the LAT catalogs.

We further analyze the *Chandra* spectra of PMN J1603–4904 and of the source to the east of PMN J1603–4904. X-ray observations by *Suzaku* and *XMM-Newton* were taken from Müller et al. (2015). The indices are consistent with the *Chandra* best fit of PMN J1603–4904, while the flux is slightly lower (see Table 2). Due to the low S/N, particularly at energies above 5 keV, the Fe emission line is not detected with *Chandra*. We model the *Chandra*/ACIS data with an absorbed powerlaw and with an absorbed collisionally-ionized emission model (APEC) and compare the results to those of the *Suzaku*/*XMM-Newton* data from 2013 (see Table 3). It is worth noting that the eastern source has a very soft index of  $\Gamma = 5.3^{+1.5}_{-2.1}$ , assuming the same absorbing column as for PMN J1603–4904. With a 21 cm derived Galactic equivalent hydrogen column of  $6.32 \times 10^{21} \text{ cm}^{-2}$  (Kalberla et al. 2005) the index is much flatter and more realistic. This suggests that the source has little or no intrinsic absorption. We add the *Chandra* data to the high-energy SED, which includes the combined *Suzaku* and *XMM* data, as well as the LAT spectrum from the 3FGL catalog (see Fig. 3). We have included both the spectrum from PMN J1603–4904 and from the eastern source (in black and pink, respectively). While it is already challenging to explain the strong  $\gamma$ -ray emission and the flat  $\gamma$ -ray index in combination with the flat X-ray index of PMN J1603–4904 (in both *Suzaku* +*XMM* and *Chandra*), it is nearly impossible to explain the soft index of the eastern source in combination with the LAT data, except by invoking different populations of particles. The high-energy SED seems to confirm that the eastern source is an extremely unlikely counterpart. Modeling the broadband SED of PMN J1603–4904 with a physical one-zone model will remain challenging with such a high Compton dominance and flat indices.

Although the optical/UV is likely non-thermal (Goldoni et al. 2016), a further possibility is thermal emission from an e.g., APEC component that would explain the He-like Fe line, which is consistent with results by Siemiginowska et al. (2016). A

**Table 3.** APEC best fit values to combined fitting of *Chandra*/ACIS and *Suzaku*/*XMM* data, and only *Suzaku*/*XMM* data. Note that the fit to the combined data sets was done using Cash statistic and not  $\chi^2$  statistics, so  $\chi^2$  is the Cash statistic value in that case.

| Fit        | $N_{\text{H}}$                | kT                  | Abundance              | $\chi^2/\text{dof}$ |
|------------|-------------------------------|---------------------|------------------------|---------------------|
|            | [ $10^{22} \text{ cm}^{-2}$ ] | [keV]               |                        |                     |
| comb.      | $1.62 \pm 0.12$               | $5.9^{+0.9}_{-0.7}$ | $0.46^{+0.16}_{-0.14}$ | 137.298/78          |
| <i>XMM</i> | $1.61 \pm 0.13$               | $6.1^{+1.1}_{-0.8}$ | $0.46^{+0.17}_{-0.16}$ | 31.816/39           |

combined fit to the *Chandra*/ACIS and combined *Suzaku* and *XMM* data results in a best fit absorbing column of  $(1.62 \pm 0.12) \times 10^{22} \text{ cm}^{-2}$ , which can explain the absence of observed He-like S/Si. It is interesting to note that this value is smaller than the value necessary for a purely phenomenological powerlaw fit with an added gaussian line, which is  $2.05^{+0.14}_{-0.12} \times 10^{22} \text{ cm}^{-2}$ . This lower value is not compatible with the Galactic absorption of  $6.32 \times 10^{21} \text{ cm}^{-2}$  and suggests intrinsic absorption, possibly from a dusty torus, which is in agreement with the interpretation of the blackbody feature in the infrared with a hot torus (Müller et al. 2014).

Photoionization is an alternative way to produce the He-like Fe emission line, but the low S/N of the spectra does not allow us to differentiate between the models.

#### 4. Conclusion

We have presented *Chandra*/ACIS and *Fermi*/LAT data of PMN J1603–4904. We show that we can rule out source confusion between the *Fermi*/LAT source and sources at lower energies by using the high angular resolution of *Chandra* and an improved 8-year localization of the  $\gamma$ -ray source 3FGL J1603.9–4903. The positional uncertainty is consistent with the radio coordinates and the X-ray counterpart. An alternative X-ray counterpart at  $\sim 1'$  distance to PMN J1603–4904 can be ruled out as a counterpart to the  $\gamma$ -ray source, based on the localization and the spectral shape. Its spectral index is further inconsistent with LAT data, as seen from the high-energy SED. Its absorbing column is consistent with Galactic absorption (although the low S/N makes a good fit of the absorbing column impossible).

Using *Chandra*/ACIS positions, fluxes, and spectra, in combination with *Fermi*/LAT data, we confirm the X-ray counterpart, rule out contributions from nearby X-ray sources, and confirm a high Compton dominance in the broadband SED of PMN J1603–4904. We therefore conclude that PMN J1603–4904 is likely one of only two known  $\gamma$ -ray emitting young radio galaxies and that its emission mechanisms and strong Compton dominance warrant further research.

*Acknowledgements.* We thank the anonymous referee for helpful comments. We thank F. D’Ammando as the internal LAT referee and A. Dominguez, E. Cavazzuti, and D. Thompson for helpful comments which have greatly improved the paper. We thank M. Hanke for the help with the projections of the TS maps. F. K. acknowledges funding from the European Union’s Horizon 2020 research and innovation program under grant agreement No 653477. C.M. acknowledges funding from the ERC Synergy Grant “BlackHoleCam: Imaging the Event Horizon of Black Holes” (Grant 545 610058). We thank J.E. Davis for the development of the `s1xfig` module that has been used to prepare the figures in this work. This research has made use of a collection of ISIS scripts provided by the Dr. Karl Remeis-Observatory, Bamberg, Germany at <http://www.sternwarte.uni-erlangen.de/isis/>. The *Fermi*-LAT Collaboration acknowledges support for LAT development, operation and data analysis from NASA and DOE (United States), CEA/Irfu and IN2P3/CNRS (France), ASI and INFN (Italy), MEXT, KEK, and JAXA (Japan), and the K.A. Wallenberg Foundation, the Swedish Research Council and the National Space Board

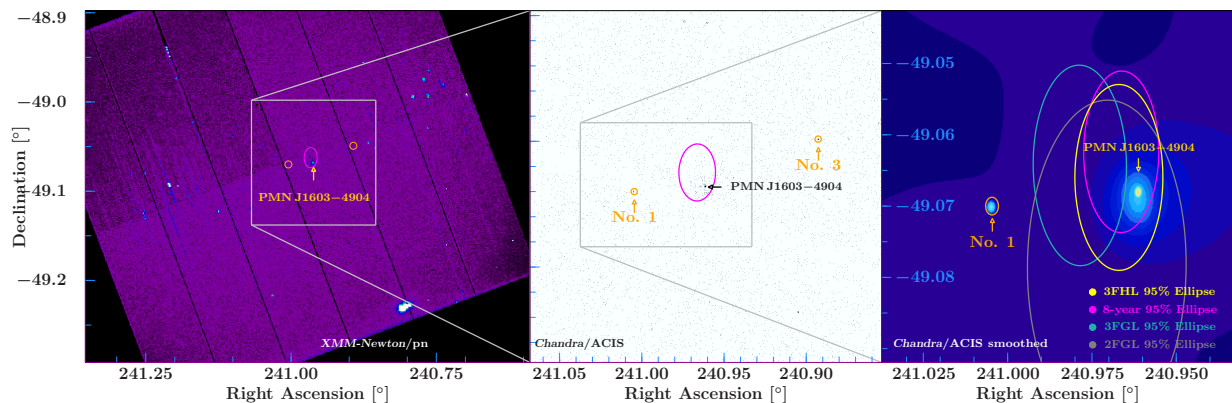


**Fig. 1.** XMM-Newton and Chandra/ACIS images of PMN J1603–4904. The positions of the sources are marked with arrows. Two unknown, weak X-ray sources are marked in orange circles. The 95% uncertainty on the *Fermi*/LAT positions from the 2FGL, 3FGL, and the 3FHL catalogs are marked in gray, green, and yellow, respectively. *Left*: XMM-Newton/pn observation (ObsID 0724700101); *Middle*: Chandra/ACIS observation (ObsID 17106); *Right*: Same Chandra/ACIS observation, the image was smoothed with a Gaussian kernel of S/N range of 3–5.

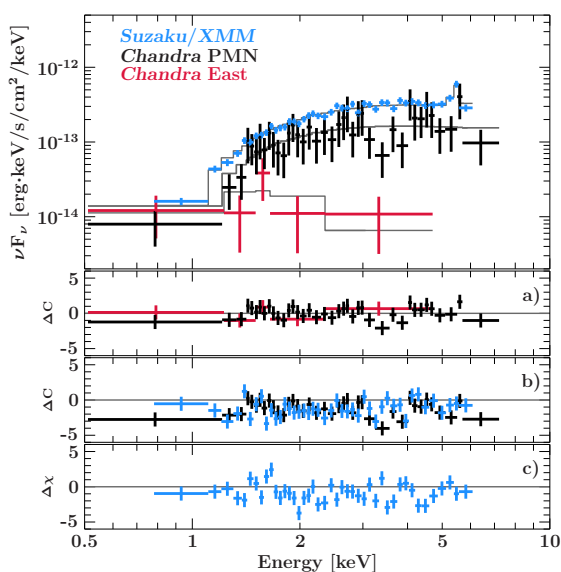


**Fig. 2.** X-ray spectra: Combined *Suzaku*/XMM-Newton spectrum of PMN J1603–4904 (blue), *Chandra*/ACIS spectrum of PMN J1603–4904 (black), *Chandra*/ACIS spectrum of the source east of PMN J1603–4904 (pink). A best-fit absorbed powerlaw is shown for the two *Chandra* spectra. The fit models shown are the best fit powerlaw models for the *Chandra* spectrum and the APEC model for the combined *Suzaku*/XMM data. Residuals are given for the a) best fit powerlaw, b) the combined APEC fit, and c) the *Suzaku*/XMM APEC fit.

(Sweden). Science analysis support in the operations phase from INAF (Italy) and CNES (France) is also gratefully acknowledged. This work performed in part under DOE Contract DE-AC02-76SF00515.

## References

Acero F., Ackermann M., Ajello M., et al., 2015, *ApJS* 218, 23  
 Ackermann M., Ajello M., Allafort A., et al., 2013, *ApJS* 209, 34  
 Ackermann M., Ajello M., Atwood W.B., et al., 2015, *ApJ* 810, 14  
 Ackermann M., Ajello M., Atwood W.B., et al., 2016, *ApJS* 222, 5  
 Atwood W., Albert A., Baldini L., et al., 2013, In: 2012 *Fermi* Symposium - eConf C121028.  
 Caccianiga A., Antón S., Ballo L., et al., 2014, *MNRAS* 441, 172  
 Cash W., 1979, *ApJ* 228, 939  
 D’Ammando F., Orienti M., Giroletti M., *Fermi* Large Area Telescope Collaboration 2016, *Astronomische Nachrichten* 337, 59

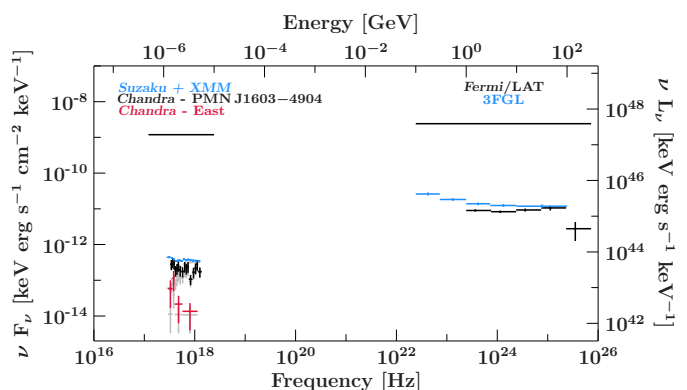


**Fig. 3.** High-energy SED showing the archival combined *Suzaku* and *XMM* data and the *Chandra*/ACIS data of both PMN J1603–4904 and the eastern source in X-rays. The *Fermi*/LAT spectrum of PMN J1603–4904 is shown. The absorbed X-ray spectra are shown in gray.

Goldoni P., Pita S., Boisson C., et al., 2016, *A&A* 586, L2  
 Gugliucci N.E., Taylor G.B., Peck A.B., Giroletti M., 2005, *ApJ* 622, 136  
 Houck J.C., Denicola L.A., 2000, In: Maset N., Veillet C., Crabtree D. (eds.) *Astronomical Data Analysis Software and Systems IX*, 216. Astronomical Society of the Pacific Conference Series, p. 591  
 Kalberla P.M.W., Burton W.B., Hartmann D., et al., 2005, *A&A* 440, 775  
 Kino M., Asano K., 2011, *MNRAS* 412, L20  
 Kino M., Ito H., Kawakatu N., Nagai H., 2009, *MNRAS* 395, L43  
 Kino M., Kawakatu N., Ito H., 2007, *MNRAS* 376, 1630  
 Kovalev Y.Y., 2009, *ApJL* 707, L56  
 Krauß F., Wilms J., Kadler M., et al., 2016, *A&A* 591, A130  
 McConville W., Ostorero L., Moderski R., et al., 2011, *ApJ* 738, 148  
 Migliori G., Siemiginowska A., Sobolewska M., et al., 2016, *ApJL* 821, L31  
 Müller C., Burd P.R., Schulz R., et al., 2016, *A&A* 593, L19  
 Müller C., Kadler M., Ojha R., et al., 2014, *A&A* 562, A4  
 Müller C., Krauß F., Dauser T., et al., 2015, *A&A* 574, A117  
 Nolan P.L., Abdo A.A., Ackermann M., et al., 2012, *ApJS* 199, 31  
 Nowak M.A., Neilsen J., Markoff S.B., et al., 2012, *ApJ* 759, 95  
 O’Dea C.P., 1998, *PASP* 110, 493  
 Orienti M., D’Ammando F., Larsson J., et al., 2015, *MNRAS* 453, 4037  
 Page M.J., Soria R., Zane S., et al., 2004, *A&A* 422, 77  
 Phillips R.B., Mutel R.L., 1982, *A&A* 106, 21  
 Predehl P., Schmitt J.H.M.M., 1995, *A&A* 293, 889  
 Readhead A.C.S., Taylor G.B., Pearson T.J., Wilkinson P.N., 1996, *ApJ* 460, 634  
 Shaw M.S., Romani R.W., Cotter G., et al., 2013, *ApJ* 764, 135  
 Siemiginowska A., Sobolewska M., Migliori G., et al., 2016, *ApJ* 823, 57  
 Skrutskie M.F., Cutri R.M., Stiening R., et al., 2006, *AJ* 131, 1163  
 Stawarz Ł., Ostorero L., Begelman M.C., et al., 2008, *ApJ* 680, 911  
 The *Fermi*-LAT Collaboration 2017, arXiv:1702.00664, accepted by *ApJS*  
 Verner D.A., Ferland G.J., Korista K.T., Yakovlev D.G., 1996, *ApJ* 465, 487  
 Wilkinson P.N., Polatidis A.G., Readhead A.C.S., et al., 1994, *ApJL* 432, L87  
 Wilks S.S., 1938, *Annals Math. Statist.* 9, 60  
 Wilms J., Allen A., McCray R., 2000, *ApJ* 542, 914  
 Wright A.E., Griffith M.R., Burke B.F., Ekers R.D., 1994, *ApJS* 91, 111